the plant journal

SEB SOCIETY FOR EXPERIMENTAL BIOLOGY

The Plant Journal (2010) **63**, 939–951 doi: 10.1111/j.1365-313X.2010.04294.x

The *male sterile 8* mutation of maize disrupts the temporal progression of the transcriptome and results in the mis-regulation of metabolic functions

Dongxue Wang[1], Juan A. Oses-Prieto[2], Kathy H. Li[2], John F. Fernandes[1], Alma L. Burlingame[2] and Virginia Walbot[1,*]
[1]*Department of Biology, 385 Serra Mall, Stanford University, Stanford, CA, 94305-5020, USA, and*
[2]*Department of Pharmaceutical Chemistry, University of California, San Francisco, CA, 94143, USA*

Received 28 May 2010; accepted 24 June 2010; published online 4 August 2010.
*For correspondence (fax 650 725 8221; e-mail walbot@stanford.edu).

SUMMARY

Maize anther ontogeny is complex, with the expression of more than 30 000 genes over 4 days of cell proliferation, cell fate acquisition and the start of meiosis. Although many male-sterile mutants disrupt these key steps, few have been investigated in detail. The terminal phenotypes of *Zea mays* (maize) *male sterile 8* (*ms8*) are small anthers exhibiting meiotic failure. Here, we document much earlier defects: *ms8* epidermal cells are normal in number but fail to elongate, and there are fewer, larger tapetal cells that retain, rather than secrete, their contents. *ms8* meiocytes separate early, have extra space between them, occupied by excess callose, and the meiotic dyads abort. Thousands of transcriptome changes occur in *ms8*, including ectopic activation of genes not expressed in fertile siblings, failure to express some genes, differential expression compared with fertile siblings and about 40% of the differentially expressed transcripts appear precociously. There is a high correlation between mRNA accumulation assessed by microarray hybridization and quantitative real-time reverse transcriptase polymerase chain reaction. Sixty-three differentially expressed proteins were identified after two-dimensional gel electrophoresis followed by liquid chromatography tandem mass spectroscopy, including those involved in metabolism, plasmodesmatal remodeling and cell division. The majority of these were not identified by differential RNA expression, demonstrating the importance of proteomics in defining developmental mutants.

Keywords: maize, *ms8,* anther, meiosis, microarray, proteomics.

INTRODUCTION

In flowering plants, pollen production first requires cell proliferation and differentiation to produce an anther, then successful completion of meiosis in a subset of centrally located anther locule cells, and finally the redifferentiation of anther somatic cells to support gametophyte maturation (Mascarenhas, 1990). These processes require coordinated gene expression among multiple cell types over 30 days in *Zea mays* (maize; Skibbe and Schnable, 2005). Maize anthers are bilaterally symmetrical, with four lobes: cells divide and differentiate within each lobe to form four distinct somatic cell types (exterior epidermis, endothecium, middle layer and innermost tapetum; Ma *et al.*, 2008) surrounding the pollen mother cells (PMCs). The tapetum plays a pivotal role in nutrient and enzyme secretion to the PMC (Goldberg *et al.*, 1993). Nuclear male sterility has been reported in many flowering plants, and in most cases mutations affect primarily tapetal or microspore development (Jung *et al.*, 2005; Xu *et al.*, 2006; Wang *et al.*, 2009).

Despite the existence of male-sterile mutants in Arabidopsis, *Solanum lycopersicum* (tomato), *Oryza sativa* (rice), maize and other species, only a few genes that control the early phases of cell proliferation, cell fate setting and initial differentiation have been identified. Furthermore, cloned genes represent diverse functions such as putative signaling pathways and metabolic enzymes, rather than a cascade of transcription factors. For example, Arabidopsis *BARELY ANY MERISTEM 1* (*BAM1*) and *BAM2* encode Leu-rich repeat receptor-like kinases: *bam1* and *bam2* mutations affect cell division and differentiation patterns, which results in the absence of endothecial, middle and tapetal layers

(Hord *et al.*, 2006). Similarly Arabidopsis *EXTRA SPOROGENOUS CELLS* (*EXS*) encodes a putative receptor thought to interact with a protein ligand encoded by *TAPETUM DETERMINANT 1* (*TPD1*; Canales *et al.*, 2002; Yang *et al.*, 2003). *GhACS1* is a cotton anther-specific acyl-CoA synthetase (ACS) required for normal fatty acid metabolism in PMC and tapetal cells. Suppression of *GhACS1* expression severely affected the tapetal cells and microsporogenesis in early anther development (Wang and Li, 2009). *Male sterile converted anther 1* (*msca1*) encodes a maize glutaredoxin (US patent no. 20090038027), in which the anther has normal morphology, but all cells differentiate as leaf cell types (Chaubal *et al.*, 2003). Normally, early leaf development genes are expressed in very immature anthers and then turned off; however, expression of these genes persists in *msca1* (Ma *et al.*, 2007). Additional genes involved in early Arabidopsis and maize anther development are summarized in Table S1.

Despite the importance of pollen in crop yield and hybrid seed production, molecular analysis of early anther development exploiting maize mutants was initiated only recently (Ma *et al.*, 2007). Maize has several advantages, primarily the large number of anthers per tassel and the lack of female floral parts in the tassel (Bedinger and Fowler, 2009). Relative to most angiosperms, maize anthers are larger, easier to dissect and cellular events are highly synchronous within each anther. Male-sterile mutants that disrupt the normal pattern of cell proliferation and differentiation prior to meiosis can be highly instructive in charting steps in cell fate acquisition and function, because specification of anther cell types is completed by the onset of meiosis. *ms8* was first recognized for meiotic failure and lack of pollen (Beadle, 1931; Albertsen and Phillips, 1981); however, anther locule cellular organization, gene expression and biochemical features have yet to be investigated. The current study was designed to quantify *ms8* defects cytologically and then to link the defects to transcriptome and proteome alterations, with the additional goal of testing whether transcriptome changes were predictive of protein abundance changes.

RESULTS

ms8 anther development

ms8 plants are indistinguishable from fertile siblings during vegetative and ear development; however, *ms8* tassels have fewer branches, anthers do not exert and no viable pollen is produced (Figure 1a). When fertile siblings shed pollen, *ms8* anthers are senescing. *ms8* anthers often adhere and cease elongating at 3.0 mm, which is about 60% of the normal final length. Dwarfing of *ms8* could reflect the early cessation of cell division and/or failure to sustain cell expansion. Scanning electron microscopy (SEM) of anthers at 3.0 mm revealed that *ms8* epidermal cells were well organized, and the number of cells was similar to that of fertile siblings. Normal epidermal cells elongate longitudinally after meiosis, and reach a length of 85 μm at the microspore stage, whereas *ms8* epidermal cells arrest at an average length of 52 μm (Figure 2b). Therefore, smaller *ms8* epidermal cells are one explanation for shorter anthers, but there is no substantial defect in longitudinal cell division.

Key stages of anther ontogeny relative to fertile anther length are summarized in Figure 1b. At 1.0 mm during rapid mitotic proliferation, there were no apparent cytological differences between *ms8* and fertile siblings (Figure 1b). At this stage there are four somatic wall layers of typical cell morphology. The endothecium and middle layers contain flattened cells elongated periclinally; neighboring tapetal cells are cuboidal with a denser cytoplasm. The presumptive PMCs at the center of each locule are encased in callose (Figure 1b). At the 1.5-mm stage, pollen mother cells partially separate and advance into meiotic prophase I in normal anthers (Figure 1b). Within *ms8* anthers there was more space between the meiocytes, and this was occupied by excess callose (Figure 1b). Normal 2.0–2.5-mm anthers had meiocytes progressing through meiosis (Figure 1b): dyads were round and intact, with no gap between the two daughter cells (Figures 1c and 2a). In contrast, *ms8* meiocytes completed the first meiotic division, but the dyads were smaller ellipsoids, with gaps between cells: the two daughter cells separated and collapsed soon afterwards (Figures 1b,c and 2a). In subsequent stages, when fertile tetrads were released and normal young microspores developed exine, intine and germ pores (Figure 1c), there was only cellular debris in the center of *ms8* locules (Figure 1b,c), indicating that meiotic cells had disintegrated.

From transverse sections (Figure S1), ~26 tapetal cells are present in 1.0-mm fertile locules, gradually increasing to ~40 (Figure 2c): only a subset of tapetal precursors present at 1.0 mm undergo subsequent mitosis. In terms of morphology, both cell thickness (diameter in the radial dimension; Figure 2d) and width (diameter within the tapetal ring; Figure 2e) were relatively constant in early stages. After meiosis, however, the normal tapetum thins and begins to degenerate (Figures 1b and 2d). Much of the dark-staining contents are secreted to coat pollen, and subsequently tapetal cells appear nearly empty. In contrast, *ms8* had only ~20 tapetal cells at the 1.0-mm stage, increasing to ~28 at the post-mitotic 1.5-mm stage. Thus, there are fewer cell divisions and an early cessation of cell division (Figure 2c), indicating a different contributing factor to the dwarf size of *ms8* anthers in this cell layer compared with the epidermis.

At the 1.0- and 1.5-mm stages, the external morphologies of *ms8* and fertile anthers are virtually identical. Maintenance of anther girth appears to reflect excessive growth of the smaller number of *ms8* tapetal cells

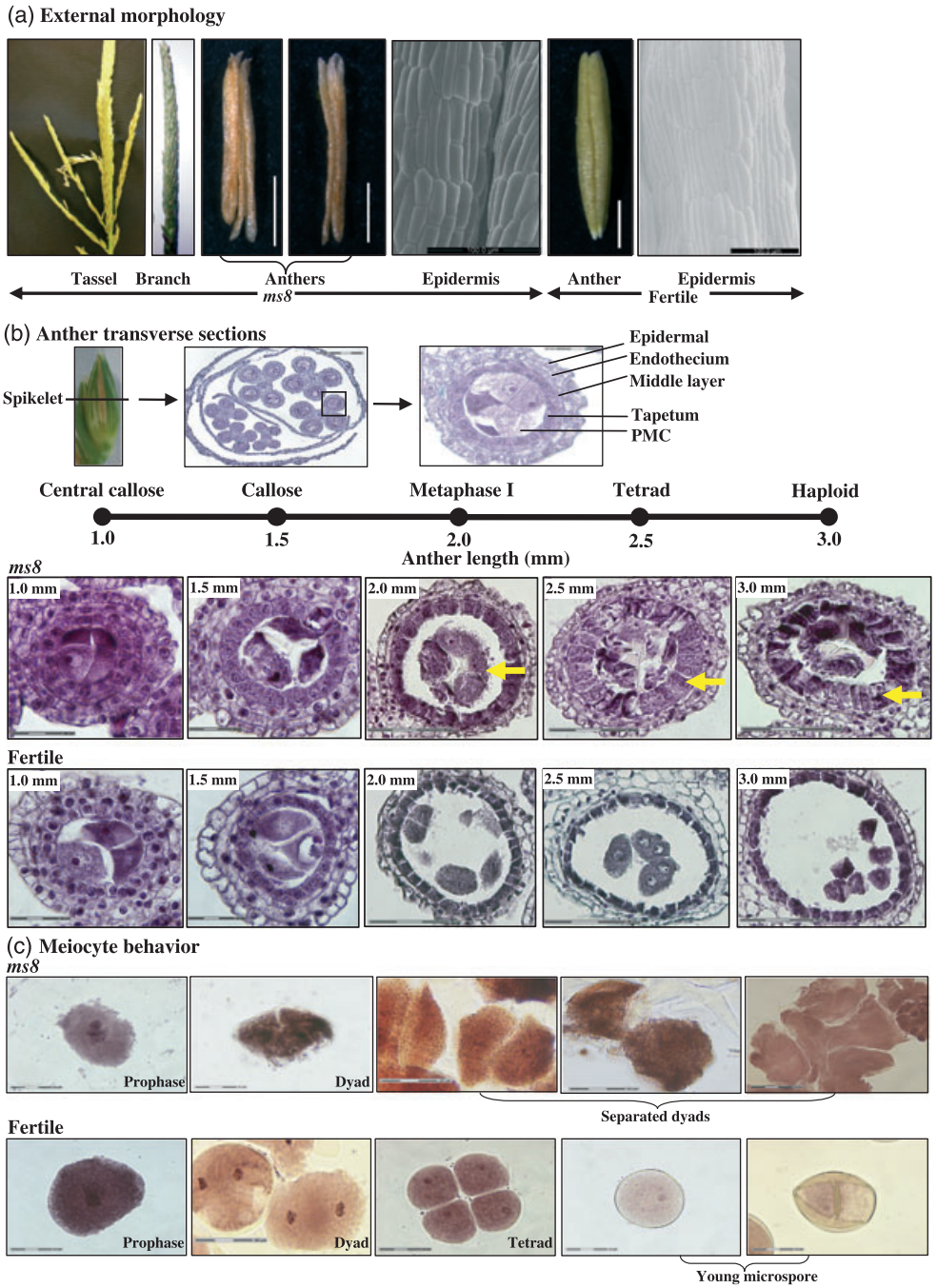

Figure 1. Phenotypic analysis of *ms8* anther locule and cell morphology.
(a) External morphology. Samples were collected from families segregating 1:1 for fertility (*ms8//+*):sterility (*ms8//ms8*). A typical *ms8* tassel is thinner and has fewer tassel branches at maturity. Dissected sterile anthers are shriveled and brown, compared with fertile anthers, which are plump and pale yellow–green. Scanning electron microscopy was used to assess epidermal cell shape and number at the 3-mm stage of *ms8* and 4-mm stage of fertile individuals. Scale bars: 1 mm (white); 100 μm (black).
(b) Each spikelet encloses two florets with three anthers each; lower floret anthers develop more slowly. There are four anther locule wall layers: epidermis, endothecium, middle layer and tapetum. pollen mother cells (PMCs) undergo meiosis, and proceed through the dyad (two cells) and tetrad (four cells) stages. During meiosis, the PMCs and product cells are normally connected by plasmodesmata. After meiosis, haploid cells normally undergo two mitotic divisions to form pollen: the microgametophyte. Anther progression is assessed by two measures: anther length and differentiation of the innermost (pre-meiotic, meiotic and then post-meiotic) cells. Cytological staging relative to maize anther length is shown above the locule photographs. Transverse sections of locules from *ms8* and from fertile plants at five developmental stages were assessed. Scale bars: 30 μm for 1.0- and 1.5-mm anther locules; 75 μm for 2.0–3.0-mm anther locules. Arrows highlight the features of *ms8* and its fertile counterpart.
(c) Meiocytes from *ms8* and from fertile anthers at different developmental stages were stained by hematoxylin-iron-aceto-carmine. *ms8* dyads were smaller, ellipsoid, separated from each other and collapsed soon after that. Scale bar: 30 μm.

(Figure S1 a1–a3). The cell length (radial diameter) was twice that of normal cells, and the cell width was slightly greater when the anther length was 2.5–3.0 mm (Figure 2d,e,g,i). Consequently, *ms8* tapetal cells are very large, occupying much of the locule space, whereas the debris from degenerating meiotic cells occupies only a small area relative to meiotic cells in fertile siblings (Figure 1b). Unlike bi-nucleate normal tapetum (Figure 2a), a majority of *ms8* tapetal cells have a single nucleus (Figure 2a). Normal tapetal cells degenerate during microspore maturation (Figures 1b and 2a), whereas mutant tapetal cells did not shrink (Figure 1b), and few degraded nuclei were found at the 3.0-mm stage (Figure 2a).

Locule transverse area was approximated by multiplying two diameter measurements. Despite the abnormalities of *ms8*, locule size (Figure 2f–h) was equivalent to fertile siblings before meiosis. Thereafter, fertile locules continued growing in girth, whereas the *ms8* mutant locule area decreased after the 2.0-mm stage. Reduced locule area was caused by extra thick tapetal cells and cell layers expansion failure. There is also a shape change: *ms8* locules are oval, but fertile locules are round (Figure 1b).

Transcriptome diversity quantified by microarray hybridization

RNA samples from fertile and sterile anthers were hybridized to custom-built Agilent 4×44 microarrays containing 42 034 probes (excluding controls) to 39 162 genes (Skibbe *et al.*, 2009). Fertile anthers exhibit astonishing transcript complexity: there are 27 400 constitutively expressed genes, 2143 stage-specific genes and 2484 genes that are expressed at two stages, giving 32 037 genes in total that are expressed over a 90-h period. This is more than 75% of the projected maize gene number. The highest diversity occurs at 1.5 mm (Figures 3a,b and S2a), confirming the results of previous studies (Ma *et al.*, 2006, 2008). Unlike these prior studies, we did not observe a 10% drop in transcript types at 2.0 mm. During the initial days of meiosis anther length is constant; hence size-based staging is not as accurate as cytology. We selected anthers at metaphase I of meiosis (Figure 1b); this narrower pooling allowed a greater depth of transcript detection than pooling 2.0-mm anthers.

As shown in Figures 3b and S2a, at 1.0 mm there are 197 stage-specific transcripts, 780 at 1.5 mm and 1166 at 2.0 mm. During the 1.0–1.5-mm transition, which spans about 72 h (Ma *et al.*, 2008), there is a major transcriptome change: 1799 new transcripts (grey checked bar in Figure 3b) and 523 transcripts expressed in the 1.0-mm anther are not detectable at 1.5 mm (black checked bar in Figure 3b). At the subsequent 1.5–2.0-mm transition, which spans about 18 h (Ma *et al.*, 2008), 326 transcripts appeared (grey checked bar in Figure 3b), 780 transcripts (black checked bar in Figure 3b) that were found at 1.5 mm disappeared, and 359 transcripts (black bar in Figure 3b) present at both the 1.0- and 1.5-mm stages are no longer detectable.

The transcriptome of *ms8* anthers is also very large: 27 284 (72%) transcripts are shared across all three *ms8* anther stages, similar to fertile siblings (Figures 3a,b and S2b). Strikingly, the 1.0-mm *ms8* anther expresses nearly 2000 more genes than fertile, and many of these are stage-specific within the context of *ms8* development (Figure 3b). Although *ms8* anthers are defective, the transcriptome is highly dynamic because new transcription factors [5% (113/2224) of the stage-specific genes] and predicted nucleic acid binding and protein binding classes are expressed. Differential expression between *ms8* and fertile siblings was evaluated using a minimum fold change of 1.5, as calculated using the LIMMA package in R (Smyth, 2005). As shown in Table S2, there are 3196 differentially regulated genes at 1.0 mm, representing the reprogramming of 11% of the normal transcriptome (3196/29 124). The significant impact of the *ms8* mutation persists through the subsequent two stages with 3748 (12%) genes differentially regulated at the 1.5-mm stage, and 3328 (11%) genes differentially regulated at the 2.0-mm meiotic stage. Among the differentially regulated transcripts at the 1.0-mm stage, *ms8* anthers had fewer downregulated (25%) than upregulated (75%) genes, whereas the opposite pattern occurs in the 1.5- and 2.0-mm stages (Table S2).

ms8 anthers develop precociously, achieving some developmental landmarks at a smaller size. Interestingly, among the 902 1.0-mm stage-specific transcripts of *ms8* anthers (grey bar in Figure 3b), 416 (46%) are expressed at later stages in normal anthers (Table S3); more than 41% (133/322) of the 1.5-mm stage-specific *ms8* transcripts are expressed at the 2.0-mm stage in fertile siblings (Table S4). Consequently, one aspect of differential gene expression in *ms8* is temporal acceleration of some transcriptome

Figure 2. Morphometric analysis of *ms8* and fertile anthers.
(a) Propidium iodide stains nuclei in meiocytes (upper panels) and tapetal cells (lower panels). *ms8* anther at 2.2-mm length, ellipsoid dyads with gaps between them (arrow); fertile locules were filled with round dyads and tetrads. The majority of *ms8* tapetal cells have a single nucleus at 2.2 mm (arrow); they remain intact and reach maximum size when anthers are 3 mm. Most fertile tapetal cells are bi-nucleate at 2.5 mm, and they have collapsed, and nuclear staining was faint, at 3 mm. Scale bars: 50 μm.
(b1) Epidermal cell dimension comparison of *ms8* and fertile anthers from 1.0 mm to 3.0 mm. (b2) Longitudinal and latitude directions are shown by arrows.
(c–g) Morphometric comparison of *ms8* and fertile anthers. (c) The number of tapetal cells. (d) Tapetal cell thickness. (e) Tapetal cell width. (f) Locule area. (g) Dimensions of the central zone internal to the tapetum.
(h) Illustration of the two measurements taken for *x* (shorter diameter) and *y* (longer diameter) at five stages in *ms8* and fertile siblings. The measurements of tapetal cell thickness and width are shown in (i) and (j), respectively. Error bars indicate standard deviations.

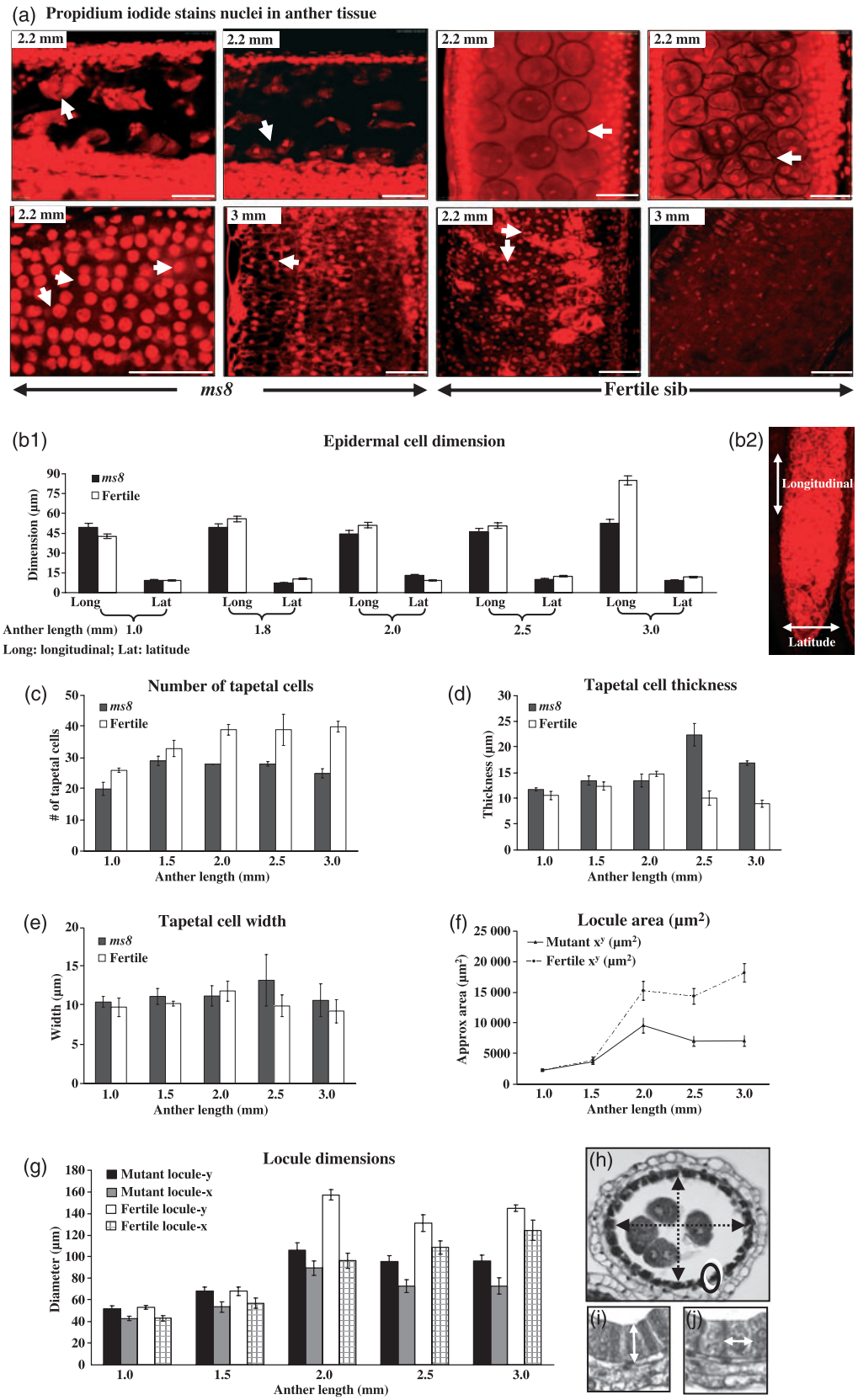

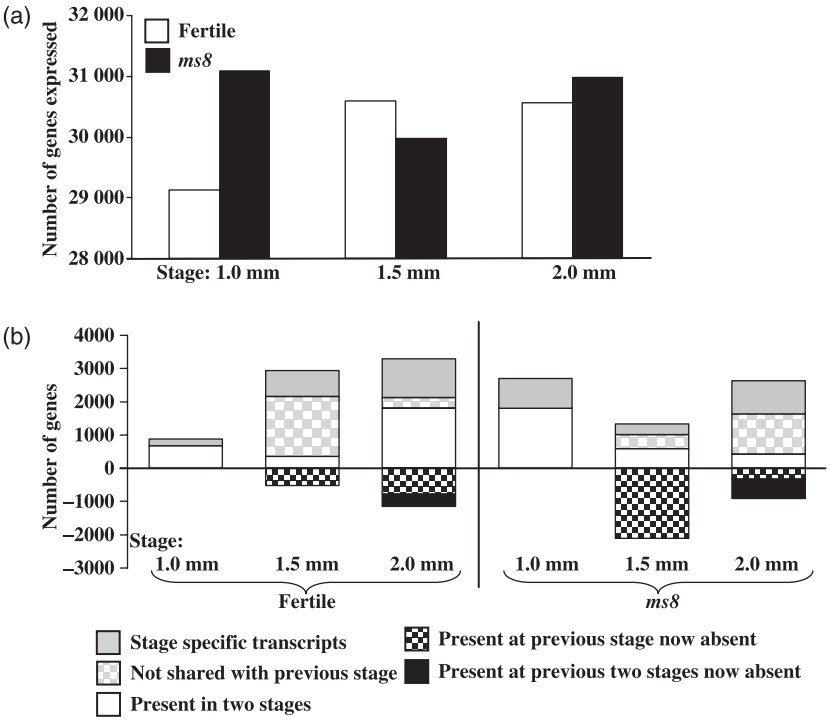

Figure 3. Transcriptome analysis of *ms8* and fertile sibling anthers.
(a) Transcriptome sizes at three stages of *ms8* and fertile sibling anthers.
(b) Analysis of transcriptome changes during fertile (left part) and sterile (right part) anther development: 27 400 transcripts shared by all stages of fertile anthers and 27 284 transcripts shared by all stages of *ms8* anthers are not shown. The *y*-axis of (a) shows the number of probes expressed, the *y*-axis of (b) shows the number of probes; the *x*-axes list the developmental stages.

programs. This is likely to disrupt the temporally coordinated growth and differentiation of *ms8* anther cells, resulting in the observed defects in cell division (tapetum) and cell elongation (epidermis).

Distinctive and shared features of transcriptome patterns of *ms8* and fertile anthers

The relationship between *ms8* and fertile anthers was further explored by *k*-means clustering. For example, among fertile genes expressed constitutively at high levels (1000-fold above the median), 150 genes in *ms8* were downregulated dramatically (on average by fourfold) in 1.5-mm anthers, but were expressed equivalently in the preceding and following stages (Figure 4a). Within this cluster are genes related to cell division, including cell division protein FtsH (TC286699) and T cytoplasm *male sterility restorer factor 2* (*Rf2*). Aniline blue staining and quantitative assays detected more callose around the mutant meiocytes at the 2.0-mm stage than in fertile siblings (Figure 5, compare c and d to g, h and i). Ninety-five genes are downregulated in the 2.0-mm *ms8* anther (Figure 4b), including β-D-glucosidase (Figure 5j), which is secreted by normal tapetum to dissolve callose (Bucciaglia and Smith, 1994). We hypothesize that excess callose accumulates because of a lack of degradation. There are 907 genes upregulated in *ms8* during the 1.5-mm stage (Figure 4c). MYB transcription factors have been identified as important in cell fate setting (Pastore *et al.*, 2008), and 10 such genes show increased expression in 1.5-mm *ms8* anthers relative to fertile anthers during the final step in cell fate setting in maize anther development (Table S5).

Zinc-finger transcription factors are among the best-studied plant DNA binding proteins, and several play important roles in floral development. In *Petunia hybrida*, seven family members were activated sequentially during anther development, and it was proposed that they might act as a regulatory cascade (Kobayashi *et al.*, 1998). Disruption of specific zinc-finger genes causes floral abnormalities, i.e. mutations in Arabidopsis *rabbit ear* (*rbe*) (Takeda *et al.*, 2004) and rice *rid1* (Wu *et al.*, 2008). Previously, 253 unique zinc-finger-related probes were examined from the maize 1.0-mm anther stage through mature pollen (Ma *et al.*, 2008), and both stage-specific and persistent expression patterns were observed. All but 28 of the 253 genes queried were expressed in at least one of the three stages examined here, and the majority (186/253 = 74%) are expressed constitutively in both *ms8* and fertile anthers (cluster 1, Figure 6). A few family members are differentially expressed: TC314427 increases 10-fold from the 1.0- to 2.0-mm stages in both fertile and *ms8* anthers (purple line, cluster 3, Figure 6). In comparing *ms8* with fertile anthers, eight zinc-finger family genes are differentially expressed in at least one stage (Table S6). Interestingly, zinc-finger transcript abundances are very diverse: they range in expression from low to moderately abundant (∼eightfold above the median, cluster 1, Figure 6) to ∼10–12-fold above the median (clusters 2 and 3), and six express at exceptionally high levels (cluster 4).

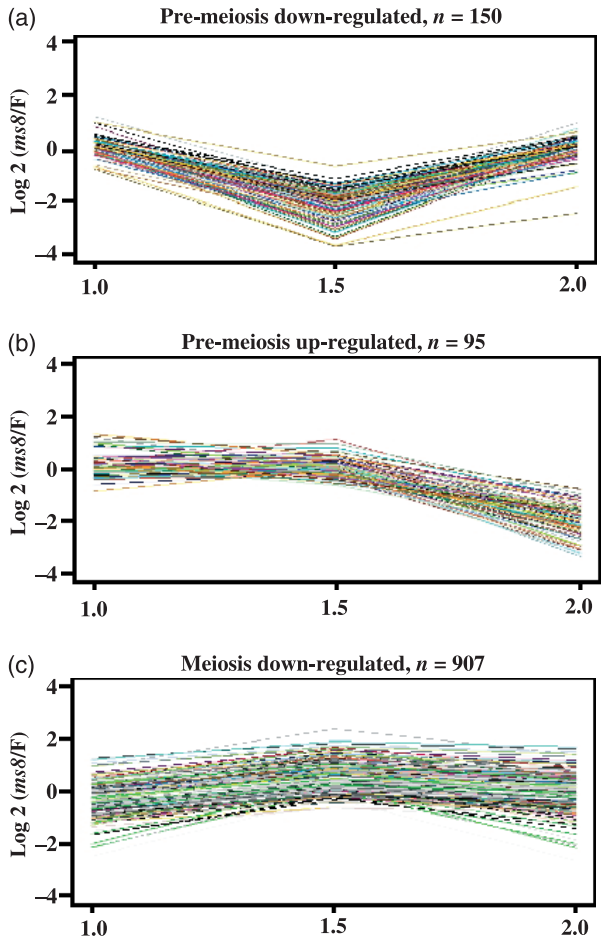

Figure 4. Differentially expressed transcripts grouped by *k*-means clustering. Transcripts constitutively expressed in fertile plants were clustered, resulting in the *ms8*/fertile fold change patterns shown: (a) 150 probes were downregulated at the 1.5-mm stage; (b) 95 probes were downregulated at the 2.0-mm stage; (c) 907 probes were upregulated at the 1.5-mm stage. The *y*-axes are the $\log_2$ ratio fold change of *ms8*/fertile. The *x*-axes show the developmental stages.

Is there mis-expression of marker genes in specific anther cell types?

Previously *msca1*, *multiple archesporial cells 1* (*mac1*) and *male sterile 23* (*ms23*) were compared with fertile siblings in 1.0–2.0-mm anthers (Ma *et al.*, 2007). All three mutants lack a cytologically normal tapetum and were missing 10 transcripts present in normal siblings: these 10 transcripts were designated tapetal marker genes. Six of these probes were queried in the current study: five had the 1.5-mm valley pattern, with a dramatic (>4-fold) decrease in *ms8* compared with normal, followed by an increase when meiosis began (Figure 7). Among them, only *TC290478* was confirmed to be expressed in epidermal and tapetal cells by laser microdissection and microarray analysis (D.S. Skibbe, personal communication): it decreased dramatically in *ms8* at the 1.5-mm stage. A sixth probe (*TC314200*) was low at the 1.0-mm stage in *ms8* relative to fertile siblings, and increased at subsequent stages, exceeding wild-type levels at the 2.0-mm stage. The *ms8* mutant has a recognizable tapetal layer, albeit with fewer cells (Figure 2c), and these cells accumulate but never secrete dark-staining material (probably protein, Figure S1 a1–a3). The array data indicate that tapetal cellular differentiation is disrupted, and the transcriptome pattern of six tapetal marker genes is abnormal at the 1.5-mm stage.

To address the contribution of an individual cell type to the distinctness of the *ms8* transcriptome, the sets of cell-type specific genes from three laser-microdissected cell types (i.e. the epidermis, tapetum and meiocytes) from 2.0-mm fertile anthers (D.S. Skibbe, personal communication) were compared with the *ms8* transcriptome. The *ms8* mutant is 96–98% similar quantitatively to a normal anther for the cell type-specific transcripts assessed (epidermis, 632 out of 659; tapetum, 451 out of 459; meiocytes, 1944 out of 2007): most differences between *ms8* and fertile siblings reflect the mis-expression of transcripts expressed in more than one cell type at 2.0 mm, rather than cell type-specific transcripts. Considered along with the measured impacts on growth in epidermal and tapetal cells it is clear that the *ms8* mutation affects multiple cell types.

Quantitative real-time reverse transcriptase polymerase chain reaction (qRT-PCR) with primers for a panel of 22 genes was used to determine the validity of specific conclusions such as constitutive expression or differential regulation of *ms8* relative to fertile plants. Sixteen constitutive genes that maintained the same quantitative expression levels across all three stages were confirmed by qRT-PCR analysis of fertile and *ms8* samples. Six genes differentially expressed in at least one stage were also consistent with the microarray data (Figure S3; Table S7).

Identification of proteins with altered abundance by two-dimensional difference gel electrophoresis (2D-DIGE) and LC/MS/MS

Anthers from the same family collected for array hybridization were used for 2D-DIGE, comparing *ms8* with normal siblings. For each stage, isoelectric focusing (IEF) was performed using two overlapping pH gradients, pH 4–7 and pH 6–11, analyzed on two different gels to increase the probability of separating proteins with similar isoelectric points. Typically, for pH 4–7 strips (24 cm), about 2700 spots were analyzed plus about 2200 spots for pH 6–11 strips (18 cm, data not shown). In the comparisons, virtually all resolved spots are yellow, indicating a similar intensity (Figure S4). Eighty-five protein spots with differential intensities of more than 1.5-fold in *ms8* from fertile comparisons were detected across the three stages: 68 were higher in *ms8* anthers and 17 were lower (data not shown). For some spots, differential expression at several stages was

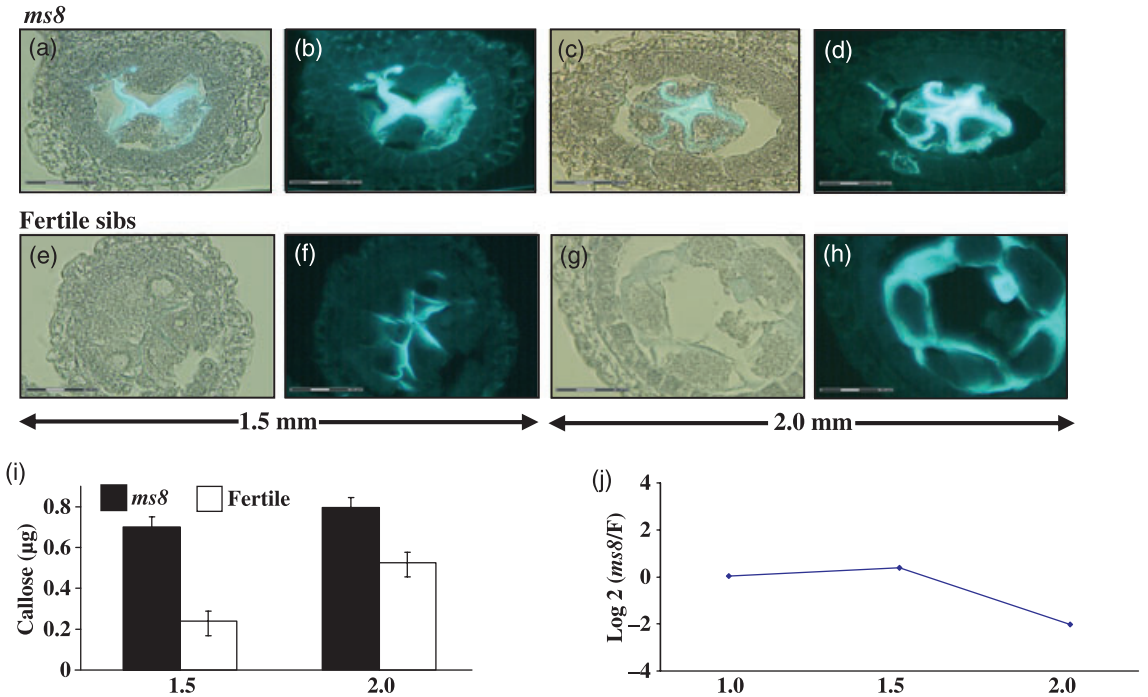

Figure 5. Aniline blue staining for callose in *ms8* and fertile sibs.
(a–d) Fluorescence in *ms8* anthers under UV illumination. (e–h) Fertile counterparts under the same UV intensity. (a, c, e and g) Bright-field and UV illumination. (b, d, f and h) UV only. (a, b, e and f) Anthers at 1.5 mm. More fluorescence was detected in *ms8* locules (a, b) than in fertile counterparts (e, f), which means excess callose surrounds *ms8* PMC. The callose occupied the extra space between separated *ms8* cells.
(c, d, g and h) Anthers at 2.0 mm. More callose surrounds the multinucleated syncytium in *ms8* locules, and no separate meiocytes were observed (c, d). The normal meiocytes were well separated and covered with a thin coat of callose (g, h).
(i) Callose comparison between *ms8* anther and fertile counterpart. The *y*-axis shows the callose level, and the *x*-axis shows two developmental stages.
(j) The expression pattern of β-D-glucosidase, an enzyme that is secreted by the tapetum to dissolve callose and release the tetrads. The *y*-axis is the fold change of *ms8*/fertile in $\log_2$ ratio, the *x*-axis shows the three developmental stages named by anther length.

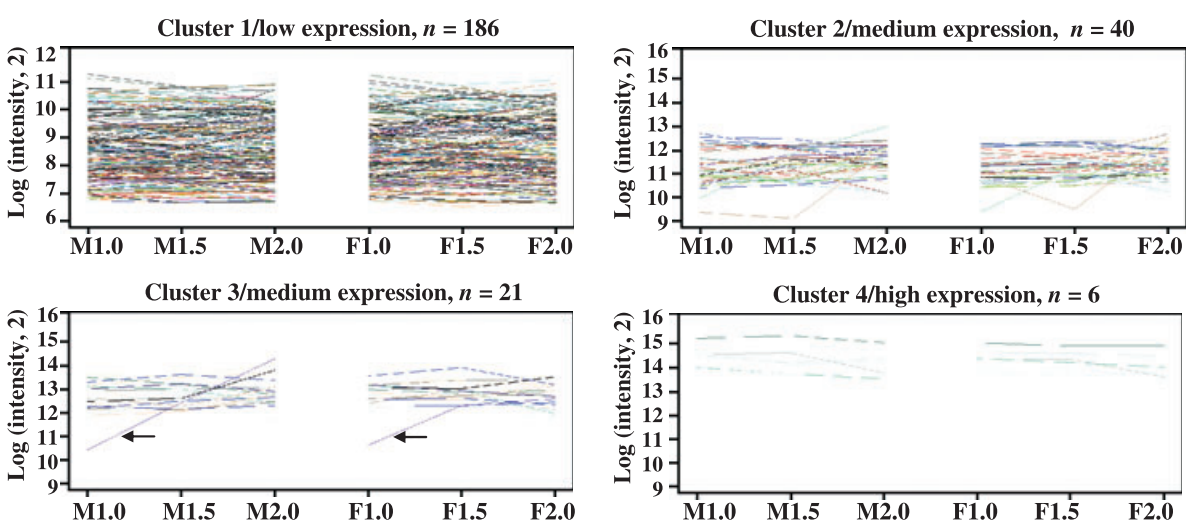

Figure 6. Clustering of zinc finger-related gene expression. Genes are sorted after *k*-means clustering (*k* = 4).
Arrows in cluster 3 show TC314427 increases 10-fold from the 1.0- to 2.0-mm stages in both fertile and *ms8* anthers. M1.0, 1.0-mm stage *ms8* anther; M1.5, 1.5-mm stage *ms8* anther; M2.0, 2.0-mm stage *ms8* anther. F1.0, 1.0-mm stage fertile anther; F1.5, 1.5-mm stage fertile anther; F2.0, 2.0-mm stage fertile anther.

detected (Table S8). After MS/MS peptide sequencing, 63 unique gene products were identified (Table S8), and functional annotations were summarized in Figure S5: proteins associated with meiosis and tapetal activities in other plants were found to be differentially expressed in *ms8* (Table S9).

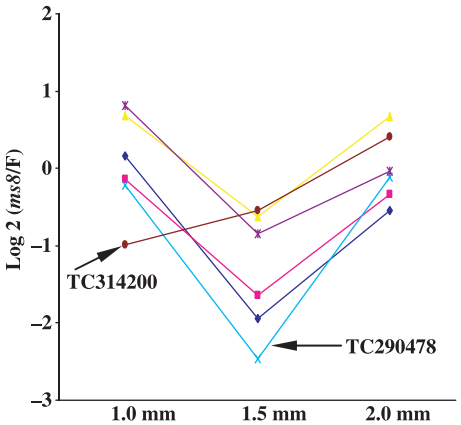

Figure 7. Expression comparison of potential cell layer markers.
Fold change pattern of previously published potential tapetum markers (Ma *et al.*, 2007), $N = 6$. The *y*-axis is $\log_2$ (fold change). The *x*-axis shows the anther developmental stages.

As observed in transcriptome studies, the highest representation of differentially expressed proteins is in metabolism: 24 proteins are upregulated and five are downregulated in *ms8* anthers (Table S8). During microsporogenesis, the tapetum supplies nutrients to sporogenous tissue (Regan and Moffatt, 1990) preceded by synthesis of free fatty acids, polar lipids, and neutral esters stored in elaioplasts and lipid bodies (Piffanelli and Murphy, 1998). ATP citrate lyase (Elshourbagy *et al.*, 1992) is critical in fatty acid synthesis and is elevated in *ms8* anthers. Two downregulated proteins are involved in amino acid metabolism: homocysteine *S*-methyltransferase-3 and cysteine synthase. Several tapetum-specific markers are cysteine-rich proteins proposed to be components of a regulatory network in young anthers (Tzeng *et al.*, 2009): synthesis of such anther-specific regulators might be affected by altered amino acid levels. Starch is synthesized in anthers before meiosis, and is subsequently hydrolyzed to provide energy for lipid synthesis in both tapetum and microspores (Vizcay-Barrena and Wilson, 2006). Aldolase 1 is also increased in *ms8* anthers, which could alter levels of sugar and starch, two molecules key to biosynthesis and energy balance. UDP-glucose-4-epimerase is higher in *ms8* anthers; this enzyme catalyzes the reversible epimerization of UDP-galactose and UDP-glucose. Elevated enzyme levels in *ms8* anthers might cause low UDP-galactose *in vivo*, and thereby affect the biosynthesis of galactose-containing cell-wall carbohydrates (Dormann and Benning, 1998). Phospholipase D increases by 2.82-fold at the 1.5-mm stage in *ms8* anthers, when mutant meiocytes have already entered prophase I. Activation of this enzyme triggers plant microtubule reorganization in both the interphase and the preprophase of mitotic cells (Dhonukshe *et al.*, 2003), hence the upregulation of this protein in *ms8* at the 1.5-mm stage could contribute to abnormal proliferation in the tapetum or aberrant features of meiosis.

Besides metabolic pathways, proper anther development requires diverse regulatory processes. 14-3-3 proteins are phosphoserine-binding proteins that regulate targets via direct protein–protein interactions, modulating among other processes plasma membrane H-ATPase, nitrate reductase, sucrose phosphate synthase and diverse cytoplasmic enzymes (Chung *et al.*, 1999). A 14-3-3-like protein (GI: 162458469) is downregulated in *ms8* 1.5-mm-stage anthers (Table S8), and another 14-3-3-like protein (GI: 226499592) was upregulated from the 1.0- to 1.5-mm stage (Figure S6; Table S8). The aberrant abundances of such 14-3-3 factors could contribute directly to *ms8* defects. In *ms8* anthers, methyl binding domain protein expression was increased before and during meiotic prophase I, and this may be related to the incipient dissolution of the PMC, as developmentally regulated DNA methylation is crucial in plants (Zemach and Grafi, 2007). Prohibitins are evolutionarily conserved proteins (Takahashi *et al.*, 2003) that play key roles in cell cycle regulation, receptor-mediated signaling at the cell surface, senescence, tumor suppression, mitochondrial function and morphology (Narasimhan *et al.*, 1997; Nadimpalli *et al.*, 2000; Chen *et al.*, 2005). There are four distinct full-length prohibitin-like genes in maize (Nadimpalli *et al.*, 2000), and both prohibitin 1 and prohibitin 4 are upregulated at the meiosis stage in *ms8* anthers (Table S8), another hallmark of dysfunction.

In eukaryotes, the spindle assembly checkpoint monitors the interaction between chromosomes and microtubules at the kinetochores, an elaborate mechanism required for correct chromosome segregation during mitosis (Caillaud *et al.*, 2009). We speculate that increased accumulation of mitotic checkpoint protein BUB3 (Table S8) in young *ms8* anthers subsequently affects spindle morphology/function in meiocytes and leads to abnormal meiosis. Phragmoplastin is a dynamin-like protein associated with cell plate formation in plants, and is encoded by eight types of maize expressed sequence tags (ESTs; data not shown). In addition to the mis-expression of mitotic checkpoint protein BUB3 that might affect phragmoplast expansion, an accumulation of excess phragmoplastin (Table S8) may also disrupt meiotic progression because these cells are normally interconnected.

Congruence of *ms8* anthers array data with proteome analysis

We compared the *ms8*-regulated proteins identified by 2D-DIGE with the *ms8*-regulated RNAs pinpointed by microarray studies (Figure S3b). Probes corresponding to only eight of the 63 identified differentially expressed proteins had differential RNA accumulation: 14-3-3-like protein (226499592), aspartate aminotransferase, translation

initiation factor 5A, protein disulfide isomerase, adenosylhomocysteinase, GTP-binding protein SAR1A, histone H2A and elongation factor 1α. For the remaining proteins, there was no significant change in RNA abundance. The small overlap between proteomics and microarray data highlights the inability of transcriptome profiling to identify changes in translational regulation, protein turnover kinetics and post-translational modification. Therefore, the proteomics assessment yielded critical additional information augmenting our understanding of the *ms8* phenotypes.

DISCUSSION

Previous studies classified *ms8* as defective in tetrad formation (Albertsen and Phillips, 1981). Based on cytological and morphometric analysis we find that *ms8* causes a dwarf anther with a cell expansion defect in the epidermis, and cell proliferation and differentiation defects in the tapetum, evident before meiosis initiates. Because excess callose is retained around the PMC and tapetal cells remain filled with material, it is likely that defective tapetal secretion starves meiotic cells, resulting in abortive meiosis. A striking feature of anther development is high transcriptome diversity, observed in maize (Ma *et al.*, 2006; this study), Arabidopsis (Wijeratne *et al.*, 2007) and rice (Jung *et al.*, 2005). The progression of gene expression programs is profoundly disrupted in *ms8* because mutants express genes atypical of normal anthers and express many genes precociously.

Analysis of cell type-specific expression indicates that most epidermal, tapetal and meiotic cell marker genes are expressed at quantitatively normal levels in *ms8* at the 2.0-mm stage. Therefore, the majority of differences between *ms8* and normal reflect the mis-expression of transcripts expressed in more than one cell type at the 2.0-mm stage. *ms23* and *ms32* are defective because presumptive tapetal cells undergo a periclinal division, forming two aberrant layers (Chaubal *et al.*, 2000): *ms8* is very distinctive from these strictly tapetal mutants in that a much higher fraction (>10%) of the *ms8* transcriptome is altered than in either tapetal mutant (~1%, Ma *et al.*, 2007; C.A. Young and V. Walbot, unpublished data). Furthermore, more than 40% of mis-expressed genes in *ms8* represent acceleration of developmental programs relative to fertile siblings. This insight indicates that precise temporal modulation is key to the progression of early anther development.

The 1.5-mm stage of *ms8* had the most significant changes compared with fertile siblings, in that transcriptome diversity was decreased, and there were the largest number of differentially expressed genes. *ms8* meiocytes cease meiosis and the tapetum is highly abnormal by the 2.0-mm stage: phenotypic consequences of mis-expression at the 1.5-mm stage 18 h earlier. We propose that the 1.5-mm stage represents a decision point for anther developmental processes, which, if aberrant, result in meiotic failure.

Mutations affecting tapetal cell size and number have been reported across a broad spectrum of flowering plants (Ma, 2005), and almost all lead to an abortive meiosis and male sterility. Arabidopsis *defective in tapetal development and function 1* (*TDF1*) expresses an anther-specific transcript that encodes a putative R2R3 MYB transcription factor, which is indirectly required for callose breakdown. From the tetrad stage, *tdf1* tapetum cells are abnormally vacuolated and enlarged, with excessive cell division (Zhu *et al.*, 2008). Mutation in rice *tapetum degeneration retardation* (*TDR*) encoding a putative basic helix-loop-helix protein caused tapetal cells to grow abnormally large, ultimately occupying the majority of the locule (Li *et al.*, 2006), as found in maize *ms8*. Both *tdf1* and *tdr* mutants have small locules of irregular shape (Li *et al.*, 2006; Zhu *et al.*, 2008), a feature shared by many other mutants (Sorensen *et al.*, 2003; Yang *et al.*, 2003; Albrecht *et al.*, 2005; Zhang *et al.*, 2006); however, locule dimension and cell count assays are available only for *ms8*, pinpointing specific defects. Meiotic failure is a routine feature among Arabidopsis mutants with tapetum developmental defects (Sorensen *et al.*, 2003; Yang *et al.*, 2003; Albrecht *et al.*, 2005; Zhang *et al.*, 2006; Zhu *et al.*, 2008): *ms8* dyads broke down and meiosis was aborted, another example connecting tapetal abnormality with meiotic failure. Transcription profiling and proteomics data are not available for *tdf* and *tdr*, or other maize anther mutants in early stages for comparison with *ms8*. Therefore, this study provides a compilation of in-depth transcriptome and proteome changes during early anther development, and will be a reference for future studies of additional mutants of maize and other species.

Callose, a β-1,3-glucan polymer with β-1,6-branches, is an insoluble polysaccharide, deposited onto the PMC at the start of meiotic prophase I. It reaches a maximum at the tetrad stage (Popova *et al.*, 2008). By aniline blue staining and quantitative analysis, *ms8* anthers accumulate more callose at the 1.5-mm stage, which occupied the extra space between PMCs, whereas at the 2.0 mm stage callose is so excessive that meiocytes are often crowded to one side of the locule. Callose accumulation appears to reflect failure of the tapetum to degrade and remodel this polysaccharide, because β-D-glucosidase is downregulated in *ms8* mutants, and no differentially regulated callose synthase genes were detected. Based on sequence homology, twelve *CALLOSE SYNTHASE* (*CalS*) genes have been identified in Arabidopsis, and five of them are required for microgametogenesis (Chen *et al.*, 2009). For example, *CalS5* encodes a callose synthase protein responsible for the temporary deposition of the callose wall surrounding microspores. *CalS5* gene knock-outs exhibit severely disrupted callose deposition and reduced fertility (Dong *et al.*, 2005). AtMYB103 is an R2R3

MYB protein that controls callose dissolution in Arabidopsis. In knock-out mutants, callose persisted into the final stages of pollen maturation: such lines are male-sterile (Zhang *et al.*, 2007). Several studies have also described mutants in callose wall formation and dissolution in petunia (Izhar and Frankel, 1971; Warmke and Overman, 1972) and tobacco (Worrall *et al.*, 1992) that disrupt fertility. Collectively, the evidence indicates that the timing of callose formation and dissolution are critical for normal fertility, and *ms8* is a new example in maize of a callose defect.

Post-meiotic tapetal cells nourish microspores and deposit complex lipoidal mixtures in tryphine or pollenkitt onto pollen (Bedinger, 1992). Several genes involved in lipid metabolism play important roles in Arabidopsis pollen development (Aarts *et al.*, 1997; Mou *et al.*, 2000). As was found in *ms8*, this class of proteins was also upregulated in the tomato *7B-1* male-sterile mutant (Sheoran *et al.*, 2009). Aberrant regulation of enzymes involved in polysaccharide (plastid starch synthase I precursor), sugar (UDP-glucose-4-epimerase, Aldolase1), and lipid metabolism are hallmarks of *ms8* and other early-acting male-sterile mutants in flowering plants. Given the significant impact of the *ms8* mutation on the transcriptome and proteome during early maize anther development, *ms8* appears to be involved in the regulation of multiple metabolic pathways.

EXPERIMENTAL PROCEDURES

Plant material and microscopy

ms8 was obtained from P. Bedinger (Colorado State University, http://www.colostate.edu) in the ND101 inbred line, and was then backcrossed four times into W23 and maintained in 1:1 segregating families (*ms8//ms8* × *ms8//+*) in summer fields at Stanford University or in glasshouses equipped with lights to replicate 50% of summer solar fluence. Samples were removed from 3 to 6-cm immature tassels by cutting through the leaf whorl; at maturity, dissected plants were scored for fertility. Only upper floret anthers were pooled from several spikelets after careful developmental staging, and then sections were prepared (Wang *et al.*, 2009) for bright-field microscopy (Axioskop 40 Pol; Carl Zeiss, http://www.zeiss.com) or stained with aniline blue (Sigma-Aldrich, http://www.sigmaaldrich.com) to visualize callose under UV illumination (Axioskop 40 Pol, DAPI channel). Callose was also quantified fluorimetrically in anther extracts (Kohle *et al.*, 1985). Meiocytes were observed by hematoxylin-iron-aceto-carmine staining (Chang and Neuffer, 1989). Scanning electron microscopy (FEI Quanta 200 scanning electron microscope; FEI Company, http://www.fei.com) images were obtained using a previously published protocol (Ohashi-Ito and Bergmann, 2006). Morphometric data were collected from four independent samples: four locules for each stage were examined, averaged and the data analyzed in EXCEL (Microsoft, http://www.microsoft.com). Propidium iodide (CalBiochem, now suuplied by Merck http://www.merck-chemicals.com) was used at 20 μg mL^{-1} in PBS solution (pH 7.4) for 30 min, with three infiltrations for 1–2 min each to stain anther nuclei for laser-scanning confocal microscopy using a Leica SP5 (Leica Microsystems Inc., http://www.leica-microsystems.com). Anther samples were imaged in water on a glass slide with a cover slip using 520–550-nm excitation and 600–650-nm emission. Cell dimension measurements were obtained from propidium iodide images, and were calculated with VOLOCITY (PerkinElmer, http://www.perkinelmer.com).

Microarray analysis and qRT-PCR assays

Total RNA was extracted with TRIzol (Invitrogen, http://www.invitrogen.com) from pools of staged anthers, and labeled cRNA was prepared as described previously by Ma *et al.* (2006) for hybridization on slides with four arrays, each of 44K elements (Agilent Technologies, http://www.agilent.com) using the Two-Color Microarray-Based Gene Expression Analysis protocol (Agilent). Four independent biological replicates at each developmental stage were analyzed with balanced dye labeling to minimize systematic variances (Table S10; Ma *et al.*, 2006; Kerr and Churchill, 2001). After hybridization according to the manufacturer's protocols, slide scanning, feature extraction, signal criterion, statistical and graphical criteria, and GO annotation were performed as described previously (Skibbe *et al.*, 2009). Normalized intensities for each probe were averaged for the four biological replicates, and the resulting final expression data and gene annotation were summarized in Table S11. The $\log_2$ of the ratio of *ms8* versus fertile sibling expression was used for clustering differentially expressed genes, as described previously (Ma *et al.*, 2008). The $\log_2$ of the normalized expression values was used for clustering the zinc-finger genes. Primer pairs (Table S7) were designed for selected genes, and then qRT-PCR reactions and amplification conditions followed published protocols (Ma *et al.*, 2008).

2D-DIGE

Protein extraction and quality assessment were performed as reported previously (Skibbe *et al.*, 2009). Three biological replicates of each developmental stage were used to identify differentially abundant spots between *ms8* and fertile siblings after labeling protein aliquots with either Cy3 or Cy5 (GE Healthcare, http://www.gehealthcare.com). Four replicates were used for microarrays, because a balanced dye swap design is required for maximal statistical power: this design feature is not required for the proteomics analysis because an internal reference containing the same proteins was included in every gel. A mixture of all samples was labeled with Cy2 (GE Healthcare) as an internal reference on all gels to improve the accuracy of quantitative comparisons (Alban *et al.*, 2003). An example of reproducibility is shown in Figure S4, utilizing a dye-swap experiment of pairs of biological replicates. Gels were scanned using a Typhoon 8600 (GE Healthcare) with appropriate wavelengths for excitation and emission (Sheoran *et al.*, 2009). Images were processed with PROGENESIS PG220 (Nonlinear Dynamics, http://www.nonlinear.com) using statistical analyses within the software. Spots with fold change of ≥1.5 or ≤−1.5 and $P < 0.05$ were considered to be differentially expressed. Aliquots (200 μg) of protein from *ms8* and its fertile counterpart plus 25 μg of each sample labeled with Cy3 or Cy5 DIGE fluor were separated on a 2D-DIGE preparative gel. The gel was fixed and stained with Deep Purple (Fluorotechnics, http://www.fluorotechnics.com), spots of interest were edited with DECYDER (GE Healthcare) and then picked by an Ettan™ spot picker (GE Healthcare). In-gel tryptic digestion was performed as described previously (Rosenfeld *et al.*, 1992, donatello.ucsf.edu/ingel.html).

Reversed-phase liquid chromatpgraphy electrospray tandem mass spectrometry (LC-MS/MS) analysis

Digests were separated by nanoflow LC as described by Oses-Prieto *et al.* (2007), with minor revisions. LTQ-FT and LTQ-Orbitrap raw

data were converted to ASCII peak lists by MASCOT DISTILLER v2.1.0.0 (Matrix Science, http://www.matrixscience.com); the parameters for MS processing were used as described previously (Oses-Prieto *et al.*, 2007). The peak lists were searched in Protein Prospector v5.3.2 (http://prospector2.ucsf.edu/prospector/html/misc/revhist.htm) (public version at http://prospector.ucsf.edu) using an existing protocol with minor updates (Deng *et al.*, 2007). The peak lists were searched using the NCBInr database as of 10 July 2009, using all entries for *Zea*, *Oryza*, *Hordeum*, *Triticum*, *Secale* and Arabidopsis (249 067 entries searched). Because the maize genome is not yet completely annotated, in some cases we relied on identification of peptides conserved in predicted proteins of plants with completely sequenced genomes (Arabidopsis and rice) or in cereals (*Triticum*, *Hordeum* and *Secale*) (Table S9). The acceptance criteria were described previously by Skibbe *et al.* (2009): only proteins with at least two peptides identified were considered further. When several accessions matched the same set of peptides, the entries with the most descriptive name were reported. Individual protein isoforms were reported when unique peptides were found; if isoforms shared peptides, they were all reported.

ACKNOWLEDGEMENTS

This research was supported by the National Science Foundation (07-01880) and the Bio-Organic Biomedical Mass Spectrometry Resource at UCSF (A.L. Burlingame, Director), supported by the Biomedical Research Technology Program of the NIH National Center for Research Resources, NIH NCRR P41RR001614 and NIH NCRR RR019934.

SUPPORTING INFORMATION

Additional Supporting Information may be found in the online version of this article:

Figure S1. Tapetal cell morphology.

Figure S2. Venn diagrams of transcriptome changes during fertile (a) and sterile (b) anther development; stage-specific transcripts and transcripts shared by two or three stages are shown respectively.

Figure S3. qRT-PCR validation of microarray and proteome data.

Figure S4. 2D-DIGE analysis of *ms8* anthers.

Figure S5. Classification of *ms8* regulated proteins based on their putative functions.

Figure S6. Increased spot I6–35 is found at both the 1.0- (left panel) and 1.5-mm stages (right panel) during *ms8* anther development.

Table S1. Genes involved in early anther development of Arabidopsis or maize with detailed phenotypic descriptions.

Table S2. Differential expressed genes, comparing *ms8* with fertile siblings.

Table S3. Four hundred and sixteen 1.0-mm stage-specific genes are expressed at a later stage in normal anthers.

Table S4. One hundred and thirty-three 1.5-mm stage-specific genes in *ms8* are expressed at the 2.0-mm stage in normal anthers.

Table S5. Ten MYB transcription factors were upregulated in *ms8* during the 1.5-mm stage.

Table S6. Eight zinc-finger family genes are differentially expressed in at least one stage.

Table S7. Primers used for qRT-PCR assays.

Table S8. *ms8* regulated proteins with maize identifiers.

Table S9. Proteins regulated by *ms8*.

Table S10. Microarray experiment design.

Table S11. Average probe intensity, final processed data, probe sequences and samples annotation.

Please note: As a service to our authors and readers, this journal provides supporting information supplied by the authors. Such materials are peer-reviewed and may be re-organized for online delivery, but are not copy-edited or typeset. Technical support issues arising from supporting information (other than missing files) should be addressed to the authors.

REFERENCES

Aarts, M.G.M., Hodge, R., Kalantidis, K., Florack, D., Wilson, Z.A., Mulligan, B.J., Stiekema, W.J., Scott, R. and Pereira, A. (1997) The Arabidopsis *MALE STERILITY 2* protein shares similarity with reductases in elongation/condensation complexes. *Plant J.* **12**, 615–623.

Alban, A., David, S.O., Bjorkesten, L., Andersson, C., Sloge, E., Lewis, S. and Currie, I. (2003) A novel experimental design for comparative two-dimensional gel analysis: two dimensional difference gel electrophoresis incorporating a pooled internal standard. *Proteomics*, **3**, 36–44.

Albertsen, M.C. and Phillips, R.L. (1981) Developmental cytology of 13 genetic male sterile loci in maize. *Genome*, **23**, 195–208.

Albrecht, C., Russinova, E., Hecht, V., Baaijens, E. and Vries, S. (2005) The *Arabidopsis thaliana* SOMATIC EMBRYOGENESIS RECEPTOR-LIKE KINASES 1 and 2 control male sporogenesis. *Plant Cell*, **17**, 3337–3349.

Beadle, G.W. (1931) Genes in maize for pollen sterility. *Genetics*, **17**, 413–431.

Bedinger, P. (1992) The remarkable biology of pollen. *Plant Cell*, **4**, 879–887.

Bedinger, P.A. and Fowler, J.E. (2009) The maize male gametophyte. In *Handbook of Maize: Its Biology* (Bennetzen, J.L. and Hake, S.C., eds). New York: Springer, pp. 57–77.

Bucciaglia, P.A. and Smith, A.G. (1994) Cloning and characterization of *Tag 1*, a tobacco anther beta-1,3-glucanase expressed during tetrad dissolution. *Plant Mol. Biol.* **24**, 903–914.

Caillaud, M.C., Paganelli, L., Lecomte, P., Deslandes, L., Quentin, M., Pecrix, Y., Bris, M.L., Marfaing, N., Abad, P. and Favery, B. (2009) Spindle assembly checkpoint protein dynamics reveal conserved and unsuspected roles in plant cell division. *PLoS ONE*, **4**, 1–9.

Canales, C., Bhatt, A.M., Scott, R. and Dickinson, H. (2002) *EXS*, a putative LRR receptor kinase, regulates male germline cell number and tapetal identity and promotes seed development in Arabidopsis. *Curr. Biol.* **12**, 1718–1727.

Chang, M.T. and Neuffer, M.G. (1989) A simple method for staining nuclei of mature and germinated maize pollen. *Biotech. Histochem.* **64**, 181–184.

Chaubal, R., Zanella, C., Trimnell, M.R., Fox, T.W., Albertsen, M.C. and Bedinger, P. (2000) Two male-sterile mutants of *Zea mays* (Poaceae) with an extra cell division in the anther wall. *Am. J. Bot.* **87**, 1193–1201.

Chaubal, R., Anderson, J.R., Trimnell, M.R., Fox, T.W., Albertsen, M.C. and Bedinger, P. (2003) The transformation of anthers in the *msca1* mutant of maize. *Planta*, **216**, 778–788.

Chen, J.C., Jiang, C.Z. and Reid, M.S. (2005) Silencing a prohibitin alters plant development and senescence. *Plant J.* **44**, 16–24.

Chen, X.Y., Liu, L., Lee, E., Han, X., Rim, Y., Chu, H., Kim, S.W., Sack, F. and Kim, J.Y. (2009) The Arabidopsis callose synthase gene *GSL8* is required for cytokinesis and cell patterning. *Plant Physiol.* **150**, 105–113.

Chung, H.J., Sehnke, P.C. and Ferl, R.J. (1999) The 14-3-3 proteins: cellular regulators of plant metabolism. *Trends Plant Sci.* **4**, 367–371.

Deng, Z., Zhang, X., Tang, W. *et al.* (2007) A proteomics study of brassinosteroid response in Arabidopsis. *Mol. Cell Proteomics*, **6**, 2058–2071.

Dhonukshe, P., Laxalt, A.M., Goedhart, J., Gadella, T.W.J. and Munnik, T. (2003) Phospholipase D activation correlates with microtubule reorganization in living plant cells. *Plant Cell*, **15**, 2666–2679.

Dong, X., Hong, Z., Sivaramakrishnan, M., Mahfouz, M. and Verma, D.P.S. (2005) Callose synthase (CalS5) is required for exine formation during microgametogenesis and for pollen viability in Arabidopsis. *Plant J.* **42**, 315–328.

Dormann, P. and Benning, C. (1998) The role of UDP-glucose epimerase in carbohydrate metabolism of Arabidopsis. *Plant J.* **13**, 641–652.

Elshourbagy, N.A., Near, J.C., Kmetz, P.J., Wells, T.N., Groot, P.H., Saxty, B.A., Hughes, S.A., Franklin, M. and Gloger, I.S. (1992) Cloning and expression of a human ATP-citrate lyase cDNA. *Eur. J. Biochem.* **204**, 491–499.

Goldberg, R.B., Beals, T.P. and Sanders, P.M. (1993) Anther development: basic principles and practical applications. *Plant Cell*, **5**, 1217–1229.

Hord, C.L.H., Chen, C., DeYoung, B.J., Clark, S.E. and Ma, H. (2006) The BAM1/BAM2 receptor-like kinases are important regulators of Arabidopsis early anther development. *Plant Cell*, **18**, 1667–1680.

Izhar, S. and Frankel, R. (1971) Mechanism of male sterility in *Petunia*: the relationship between pH, callase activity in the anthers, and the breakdown of the microsporogenesis. *Theor. Appl. Genet.* **41**, 104–108.

Jung, K.H., Han, M.J., Lee, Y.S., Kim, Y.W., Hwang, I., Kim, M.J., Kim, Y., Nahm, B.H. and An, G. (2005) Rice *Undeveloped Tapetum1* is a major regulator of early tapetum development. *Plant Cell*, **17**, 2705–2722.

Kerr, M.K. and Churchill, G.A. (2001) Statistical design and the analysis of gene expression microarray data. *Genet. Res.* **77**, 123–128.

Kobayashi, A., Sakamoto, A., Kubo, K., Rybka, Z., Kanno, Y. and Takatsuji, H. (1998) Seven zinc finger transcription factors are expressed sequentially during the development of anthers in petunia. *Plant J.* **13**, 571–576.

Kohle, H., Jeblick, W., Poten, F., Blaschek, W. and Kauss, H. (1985) Chitosan-elicited callose synthesis in soybean cells as a Ca^{2+}-dependent process. *Plant Physiol.* **77**, 544–551.

Li, N., Zhang, D.S., Liu, H.S. *et al.* (2006) The rice *tapetum degeneration retardation* gene is required for tapetum degradation and anther development. *Plant Cell*, **18**, 2999–3014.

Ma, H. (2005) Molecular genetic analyses of microsporogenesis and microgametogenesis in flowering plants. *Annu. Rev. Plant Biol.* **56**, 393–434.

Ma, J., Morrow, D.J., Fernandes, J. and Walbot, V. (2006) Comparative profiling of the sense and antisense transcriptome of maize lines. *Genome Biol.* **7**, doi: 10.1186/gb-2006-7-3-r22.

Ma, J., Duncan, D., Morrow, D.J., Fernandes, J. and Walbot, V. (2007) Transcriptome profiling of maize anthers using genetic ablation to analyze premeiotic and tapetal cell type. *Plant J.* **50**, 637–648.

Ma, J., Skibbe, D.S., Fernandes, J. and Walbot, V. (2008) Male reproductive development: gene expression profiling of maize anther and pollen ontogeny. *Genome Biol.* **9**, doi: 10.1186/gb-2008-9-12-r181.

Mascarenhas, J.P. (1990) Gene activity during pollen development. *Annu. Rev. Plant Physiol.* **41**, 317–338.

Mou, Z., He, Y., Dai, Y., Liu, X. and Li, J. (2000) Deficiency in fatty acid synthase leads to premature cell death and dramatic alterations in plant morphology. *Plant Cell*, **12**, 405–417.

Nadimpalli, R., Yalpani, N., Johal, G.S. and Simmons, C.R. (2000) Prohibitins, stomatins, and plant disease response genes compose a protein superfamily that controls cell proliferation, ion channel regulation, and death. *J. Biol. Chem.* **275**, 29579–29586.

Narasimhan, S., Armstrong, M., McClung, J.K., Richards, F.F. and Spicer, E.K. (1997) Prohibitin, a putative negative control element present in *Pneumocystic carinii. Infect. Immun.* **65**, 5125–5130.

Ohashi-Ito, K. and Bergmann, D.C. (2006) Arabidopsis FAMA controls the final proliferation/differentiation switch during stomatal development. *Plant Cell*, **18**, 2493–2505.

Oses-Prieto, J.A., Zhang, X. and Burlingame, A.L. (2007) Formation of ∈-formyllysine on silver-stained proteins. *Mol. Cell Proteomics*, **6**, 181–192.

Pastore, J., Chavdaroff, N. and Wagner, D. (2008) LMI2, a MYB transcription factor involved in the vegetative to reproductive transition in *Arabidopsis thaliana. Dev. Biol.* **319**, 565–575.

Piffanelli, P. and Murphy, D.J. (1998) Novel organelles and targeting mechanisms in the anther tapetum. *Trends Plant Sci.* **3**, 250–253.

Popova, A.F., Ivanenko, G.F., Ustinova, A.Y. and Zaslavsky, V.A. (2008) Localization of callose in microspores and pollen grains in *Sium latifolium* L. plants in different water regimes. *Cytol. Genet.* **42**, 363–368.

Regan, S.M. and Moffatt, B.A. (1990) Cytochemical analysis of pollen development in wild-type Arabidopsis and a male-sterile mutant. *Plant Cell*, **2**, 877–889.

Rosenfeld, J., Capdeveille, J., Guillemot, J.C. and Ferrara, P. (1992) In-gel digestion of proteins for internal sequence analysis after one- or two-dimensional gel electrophoresis. *Anal. Biochem.* **203**, 173–179.

Sheoran, I.S., Ross, A.R.S., Olson, D.J.H. and Sawhney, V.K. (2009) Differential expression of proteins in the wild type and *7B-1* male-sterile mutant anthers of tomato (*Solanum lycopersicum*): a proteomic analysis. *J. Proteomics*, **71**, 624–636.

Skibbe, D.S. and Schnable, P.S. (2005) Male sterility in maize. *Maydica*, **50**, 367–376.

Skibbe, D.S., Fernandes, J.F., Medzihradszky, K.F., Burlingame, A.L. and Walbot, V. (2009) Mutator transposon activity reprograms the transcriptomes and proteomes of developing maize anthers. *Plant J.* **59**, 622–633.

Smyth, G.K. (2005) Limma: linear models for microarray data. In *Bioinformatics and Computational Biology Solutions using R and Bioconductor* (Gentleman, R., Carey, V., Dudoit, S., Irizarry, R. and Huber, W., eds). New York: Springer, pp. 397–420.

Sorensen, A.M., Kröber, S., Unte, U.S., Huijser, P., Dekker, K. and Saedler, H. (2003) The Arabidopsis *ABORTED MICROSPORES* (*AMS*) gene encodes a MYC class transcription factor. *Plant J.* **33**, 413–423.

Takahashi, A., Kawasaki, T., Wong, H.L., Suharsono, U., Hirano, H. and Shimamoto, K. (2003) Hyperphosphorylation of a mitochondrial protein, prohibitin, is induced by calyculin A in a rice lesion-mimic mutant *cdr1*. *Plant Physiol.* **132**, 1861–1869.

Takeda, S., Matsumoto, N. and Okada, K. (2004) *RABBIT EARS*, encoding a superman-like zinc finger protein, regulates petal development in *Arabidopsis thaliana*. *Development*, **131**, 425–434.

Tzeng, J.D., Hsu, S.W., Chung, M.C., Yeh, F.L., Yang, C.Y., Liu, M.C., Hsu, Y.F. and Wang, C.S. (2009) Expression and regulation of two novel anther-specific genes in *Lilium longiflorum*. *J. Plant Physiol.* **166**, 417–427.

Vizcay-Barrena, G. and Wilson, Z.A. (2006) Altered tapetal PCD and pollen wall development in the Arabidopsis *ms1* mutant. *J. Exp. Bot.* **57**, 2709–2717.

Wang, X.L. and Li, X.B. (2009) The GhACS1 gene encodes an acyl-CoA synthetase which is essential for normal microsporogenesis in early anther development of cotton. *Plant J.* **57**, 473–486.

Wang, D., Li, C., Zhao, Q., Zhao, L., Wang, M., Zhu, D., Ao, G. and Yu, J. (2009) *Zm401p10*, encoded by an anther-specific gene with short open reading frames, is essential for tapetum degeneration and anther development in maize. *Funct. Plant Biol.* **36**, 73–85.

Warmke, H.E. and Overman, M.A. (1972) Cytoplasmic male sterility in sorghum. I. Callose behavior in fertile and sterile anthers. *J. Hered.* **63**, 103–108.

Wijeratne, A.J., Zhang, W., Sun, Y., Liu, W., Albert, R., Zheng, Z., Oppenheimer, D., Zhao, D. and Ma, H. (2007) Differential gene expression in Arabidopsis wild-type and mutant anthers: insights into anther cell differentiation and regulatory networks. *Plant J.* **52**, 14–29.

Worrall, D., Hird, D.L., Hodge, R., Paul, W., Draper, J. and Scott, R. (1992) Premature dissolution of the microsporocyte callose wall causes male sterility in transgenic tobacco. *Plant Cell*, **4**, 759–771.

Wu, C., You, C., Li, C., Long, T., Chen, G., Byrne, M.E. and Zhang, Q. (2008) *RID*1, encoding a Cys2/His2-type zinc finger transcription factor, acts as a master switch from vegetative to floral development in rice. *Proc. Natl Acad. Sci. USA*, **105**, 12915–12920.

Xu, S.X., Liu, G.S. and Chen, R.D. (2006) Characterization of an anther- and tapetum-specific gene and its highly specific promoter isolated from tomato. *Plant Cell Rep.* **25**, 231–240.

Yang, S.L., Xie, L.F., Mao, H.Z., Puah, C.S., Yang, W.C., Jiang, L., Sundaresan, V. and Ye, D. (2003) The *TAPETUM DETERMINANT1* gene is required for cell specialization in the Arabidopsis anther. *Plant Cell*, **15**, 2792–2804.

Zemach, A. and Grafi, G. (2007) Methyl-CpG-binding domain proteins in plants: interpreters of DNA methylation. *Trends Plant Sci.* **12**, 1380–1385.

Zhang, W., Sun, Y., Timofejeva, L., Chen, C., Grossniklaus, U. and Ma, H. (2006) Regulation of Arabidopsis tapetum development and function by *DYSFUNCTIONAL TAPETUM1* (*DYT1*) encoding a putative bHLH transcription factor. *Development*, **133**, 3085–3095.

Zhang, Z.B., Zhu, J., Gao, J.F. *et al.* (2007) Transcription factor *AtMYB103* is required for anther development by regulating tapetum development, callose dissolution and exine formation in Arabidopsis. *Plant J.* **52**, 528–538.

Zhu, J., Chen, H., Li, H., Gao, J.F., Jiang, H., Wang, C., Guan, Y.F. and Yang, Z.N. (2008) *Defective in tapetal development and function 1* is essential for anther development and tapetal function for microspore maturation in Arabidopsis. *Plant J.* **55**, 266–277.

